

Optical Tomographic Imaging of Tumor Hemodynamics during Anti-VEGF Treatment in Mice

James Masciotti¹, Frank Provenzano¹, Joey Papa³, Junho Hur¹, Xuejun Gu¹, Qi Wu¹, Alexander Klose¹, Darrell Yamashiro³, Jessica Kandel³, Andreas H. Hielscher^{1,2}

¹Department of Biomedical Engineering, Columbia University, 351 Engineering Terrace., 500 West 120th St., New York, NY 10027

²Department of Radiology, Columbia University, 660 West 168th St., New York, New York 10327

³Department of Pediatrics and Surgery, Columbia University, 1130 St. Nicholas Ave., Room 217, New York, NY 10027

e-mail: ahh2004@columbia.edu

Abstract: We use dynamic optical tomographic imaging methods to monitor immediate effects of an injectable anti-VEGF treatment. As early as 8 minutes after the drug is administered, measurable changes can be observed, which herald long-term vascular destruction.

©2003 Optical Society of America

OCIS codes: (170.3880) Medical and Biological Imaging; (170.6960) Tomography

1. Introduction

Over the past decade considerable effort has been put into the development of small animal imaging systems. This work has been motivated by advances in animal models of human diseases and the progress in their transgenic manipulation [1,2]. The goal of many of these novel imaging systems is to noninvasively monitor the temporal as well as spatial progression of disease and other biological processes. Optical imaging techniques have shown great promise in this regard. Though offering poorer spatial resolution than, for example, micro CT or magnetic resonance imaging (MRI), optical methods can be used to measure physiologically important chromophore concentrations such as oxyhemoglobin (HbO₂) and deoxyhemoglobin (Hb) with high temporal resolution [2-4]. Furthermore, optical methods are also sensitive to blood volume changes, scattering properties, and can be used in combination with molecular markers [5]. Temporal resolution in the range of 1 Hz to 50 Hz can be achieved relatively easily, allowing for relatively fast completion of complex imaging protocols. One promising application is the monitoring of hemodynamic effects during cancer treatment in mouse models. For example, we have used optical tomography combined with magnetic resonance imaging (MRI) to monitor regression of tumors in mice after treatment with a vascular endothelia growth factor (VEGF) antagonist [7,8]. We found that reduction in blood volume can be observed as early as 24 hours after treatment, when anatomical changes are not yet visible in MR images. This finding was in agreement with other studies that have shown disrupting VEGF signaling, which is responsible for angiogenesis, and can attenuate or even abolish tumor vasculature, producing marked tumor regression [9,10]. The exact mechanisms by which the chemotherapy destroys blood vessels in the tumor and causes its regression is not completely understood. Of special interest here is the early onset of the drug-tissue interaction. Making use of the unique features of dynamical optical tomography, we continuously image in the study at hand tumor bearing mice from 5 minutes before to 50 minutes after drug injection.

2. Methods

2.1 Mouse Tumor Model

We orthotopically implanted kidney tumor cells in 10 NCR athymic nude mice. Tumors were allowed to grow for 52 days, during which the growth was monitored with MRI (Fig. 1a) once a week and with optical tomography, twice a week. On the 52nd day a treatment schedule consisting of 0.1 cc anti-VEGF injections twice a week was begun. Optical tomographic data sets were obtained every 0.4 s from 5 minutes before until 50 minutes after drug injection. Before the imaging session the animal was anesthetized with ketamine and one end of a thin cannula (PE-10) was inserted into the intraperitoneal cavity. The other end was attached to a needle on a 0.5 cc syringe filled with the VEGF antagonist. In this way the treatment could be administered during the optical scan without removing the animal from the optical imaging probe. In addition to these dynamic studies, optical tomographic images were obtained 24 and 96 hours after the injection.

2.2 Optical Imaging Instrument and Measurement Head

For the optical tomographic measurements we employed a continuous wave mode, dynamic near-infrared optical tomographic (DYNOT) instrument [10]. The fibers of the DYNOT instrument was coupled to an optical imaging probe consisting of a hollow Delrin cylinder (diameter = 5cm, height = 10 cm) and two fiber-holding rings, which allow the ends of the fibers to be in contact with the surface of the cylinder and can be slid up and down the cylinder

to adjust the vertical position of the fibers. Each of the 2 rings had 24 holes drilled, spaced 15° apart allowing 12 source and 12 detector fibers arranged in an alternating pattern for a total of 24 sources, 24 detectors and thus 576 source detector pairs (see Fig. 1b). 2.5 full tomographic dataset per seconds, involving all 576 source-detector pair readings of light intensity, were acquired.

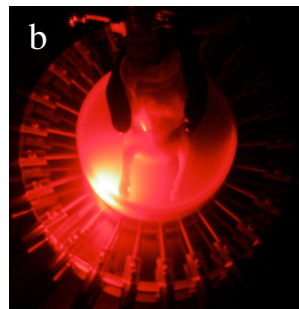


Fig. 1. T2 weighted MR image (a) showing large tumor (the bright mass) of mouse that was given the treatment scan and a photograph (b) of a mouse in the experimental set-up consisting of 24 sources and 24 detectors

The cylinder was partially filled with 1% Intralipid which was used as a matching fluid in order to reduced edge effects during image reconstruction. The 1% Intralipid was obtained by diluting 10% Intralipid (Sigma-Aldrich Corp. St. Louis, MO). The mouse was fixed in an anesthesia nose cone which was suspended from a stereotaxic frame and allowed the mouse to be lowered into the cylinder. Before placement in the optical probe the syringe was stabilized on a surface so that the treatment injection could be administered through the cannula with causing minimal movement inside the probe. The rings, separated by 1.3 cm, were adjusted so that the tumor was in between the two rings. After the mouse was placed in the probe, the optimal detector gain settings were found for each source detector pair. Subsequently the optical scan was performed continuously for approximately 50 minutes.

3. Results

Fig. 2 shows a time series trace of the light detected for one representative source detector pair. The treatment was administered 4 minutes into the scan at time 0. A small signal decrease occurs from 6 to 9 minutes. A steep sustained signal increase begins just after the dip at 9 minutes and remains for the remainder of the experiment, but becomes more gradual after 20 minutes.

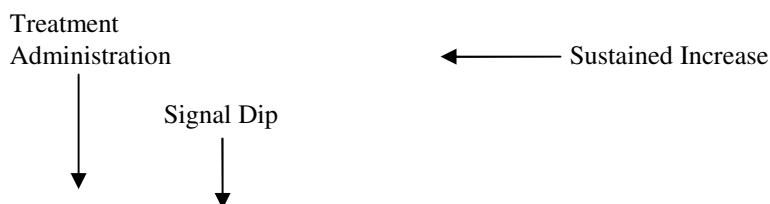


Fig 2. Time trace of measured light intensity for an example source detector pair.

From the 55 minute time-series data, blocks of 400 points (160 s) were taken and averaged at the beginning of the experiment and then every 4 minutes starting immediately after injection. This data was input into a model-based iterative reconstruction (MOBIR) algorithm based on a finite difference implementation of the time-independent equation of radiative transfer [11]. Examples of reconstructed absorption images are presented in fig. 3. The large circular shape corresponds to the cylinder cross-section. Small areas of high absorption on the edge of the circle are source boundary artifacts. The mouse was located with back against the rear of the cylinder (top of image). Figs. 3a-3e shows the absorption coefficient image for the mouse at various time points from just prior to injection to 32 minutes after injection. The area of high absorption is collocated with the tumor as confirmed with MRI. Figs. 3f-3j show images that represent the original absorption image (3a) minus the absorption images at each of the various time points. At 8 minutes after drug injection (Figs. 3c and 3h) one can observe a decrease in absorption around the periphery of the tumor and an increase in absorption inside the tumor. A decrease in the absorption coefficient inside the tumor occurs there after. By 32 minutes after injection a large decrease in

absorption coefficient is observed inside the tumor. In most cases we observed that this or an even stronger decrease is still present 24 hours after treatment.

f) g) h) i) j)

Fig. 3. Maps of the absorption coefficient (in units of cm^{-1}) for (a) 0, (b) 4, (c) 8, (d) 16, and (e) 32 minutes after injection; and changes in absorption coefficient, with respect to Fig. 3a, for (f) 0, (g) 4, (h) 8, (i) 16, and (j) 32 minutes after injection.

4. Discussion and Conclusion

Using optical tomography we studied the immediate effects of a VEGF antagonist on tumor vasculature in a mouse model. We observed an effect as early as eight minutes after administration of the drug. After a short increase in absorption in the center of the tumor, we observe a sustained decrease in absorption, which we believe corresponds to a decrease in tumor blood volume. We believe this drop in blood volume is most likely due to the fact that blocking VEGF causes a decrease in nitric oxide, which in turn leads to vessel constriction. This immediate decrease in tumor blood volume is different from vascular destruction, which is known to begin 24 hours after treatment, and is known to cause tumor regression. Dual-wavelength studies are currently underway that will allow calculations of changes in Hb and HbO_2 concentration. This information will aid in further understanding of the observed early effects during VEGF antagonist treatment.

This work was supported in part by the National Institute of Biomedical Imaging and Bioengineering (NIBIB grant 5R01-EB001900, Hielscher) and the National Cancer Institute (NCI grants 5R01CA100451, Kandel, and 5R01CA088951, Yamashiro), which both are divisions of the National Institutes of Health (NIH).

5. References

- [1] M. G. Pomper, "Can small animal imaging accelerate drug development?," *J. Cell. Biochem. Suppl.* **39**, pp. 211-220. (2002).
- [2] A.H. Hielscher, "Optical tomographic imaging of small animals," *Current Opinion in Biotechnology* **16**(1), pp. 79-88 (2005)
- [3] A. Y. Bluestone, M. Stewart, B. Lei, I.S. Kass, J. Lasker, G.S. Abdoulaev, A. H. Hielscher, "Three-dimensional optical tomographic brain imaging in small animals, Part I: Hypercapnia & Part II: Unilateral Carotid Occlusion," *J. Biomedical Optics* **9**(5), pp. 1046-1173 (2004).
- [4] J. P. Culver, T. Durduran, D. Furuya, C. Cheung, J. H. Greenberg, A. G. Yodh, "Diffuse optical tomography of cerebral blood flow, oxygenation, and metabolism in rat during focal ischemia," *J. of Cerebral Blood Flow & Metabolism* **23**, pp. 911-924 (2003).
- [5] E. E. Graves, R. Weissleder, V. Ntzachristos, "Fluorescence Molecular Imaging of Small Animal Tumor Models," *Current Molecular Medicine* **4**, pp. 419-430 (2004).
- [6] J. Masciotti, G. Abdoulaev, J. Hur, J. Papa, J. Bae, J. Huang, D. Yamashiro, J. Kandel, A.H. Hielscher, "Combined optical tomographic and magnetic resonance imaging of tumor bearing mice," in *Optical Tomography and Spectroscopy of Tissue VII*, B. Chance, R.R. Alfano, B.J. Tromberg, M. Tamura, E.M. Sevick-Muraca, eds., Proc. 5693, pp. 74-81 (2005).
- [7] J. Masciotti, G. Abdoulaev, F. Provenzano, J. Hur, J. Papa, J. Bae, J. Huang, D. Yamashiro, J. Kandel, and A. H. Hielscher, "Optical Tomographic and Magnetic Resonance Imaging of Tumor Growth and Regression in Mice with VEGF Blockade," *27th Annual International Conference of the IEEE Engineering in Medicine and Biology Society*, (Institute of Electrical and Electronics Engineers, Shanghai, 2005)
- [8] J. Glade-Bender, J. J. Kandel, D. J. Yamashiro, "VEGF blocking therapy in the treatment of cancer," *Expert Opin. Bio. Therapy* **3**(2), pp. 263-276 (2003).
- [9] J. S. Frischer, J. Z. Huang, A. Serur, A. Kadenhe-Chiweshe, K. W. McCrudden, K. O'Toole, J. Holash, G. D. Yancopoulos, D. J. Yamashiro, J. J. Kandel, "Effects of potent VEGF blockade on experimental Wilms tumor and its persisting vasculature," *Int. J. Oncology* **25**(3), pp. 549-553 (2004).
- [10] C.H. Schmitz, M. Löcker, J. M. Lasker, A. H. Hielscher, R. L. Barbour, "Instrumentation for fast functional optical tomography," *Review of Scientific Instrumentation* **73**(2), pp. 429-439 (2002).
- [11] A. K. Klose, V. Ntzachristos, A.H. Hielscher, "The inverse source problem based on the radiative transfer equation in molecular optical imaging," *J. Computational Physics* **202**, pp. 323-345 (2005).